

Sensing of single nuclear spins in random thermal motion with proximate nitrogen-vacancy centers

M. Bruderer, P. Fernández-Acebal, R. Aurich and M. B. Plenio

Institut für Theoretische Physik, Albert-Einstein Allee 11, Universität Ulm, 89069 Ulm, Germany

Nitrogen-vacancy (NV) centers in diamond have emerged as valuable tools for sensing and polarizing spins. Motivated by potential applications in chemistry, biology and medicine we show that NV-based sensors are capable of detecting single spin targets even if they undergo diffusive motion in an ambient thermal environment. Focusing on experimentally relevant diffusion regimes we derive an effective model for the NV-target interaction, where parameters entering the model are obtained from numerical simulations of the target motion. The practicality of our approach is demonstrated by analyzing two realistic experimental scenarios: (i) time-resolved sensing of a fluorine nuclear spin bound to an N-heterocyclic carbene-ruthenium (NHC-Ru) catalyst that is immobilized on the diamond surface and (ii) detection of an electron spin label by an NV center in a nanodiamond, both attached to a vibrating chemokine receptor in thermal motion. We find in particular that the detachment of a fluorine target from the NHC-Ru carrier molecule can be monitored with a time resolution of a few seconds.

PACS numbers: 76.70.Hb, 75.75.Lf, 76.60.Lz

I. INTRODUCTION

Single-molecule observation techniques have provided many important insights into the details of fundamental chemical and biological processes. Specifically, the investigation of single-molecule catalytic reactions in various environments has been made possible by several, primarily spectroscopic methods. To give some examples, fluorescence microscopy has been used to observe single-molecule enzymatic dynamics [1–3] and to determine the spatial distribution of catalytic activity on crystal surfaces [4]. Moreover, scanning tunneling microscopy has demonstrated its potential for monitoring oxidation catalysis in real time at liquid-solid interfaces [5].

More recently, nitrogen-vacancy (NV) centers in bulk diamond [6] have been used for spin resonance spectroscopy with a sensitivity ultimately reaching the single-molecule level [7–9], which makes them a promising new tool for probing the dynamics of chemical processes. This is particularly true for single-site catalytic reactions [10], in which case the catalyst is immobilized on a surface while maintaining its full catalytic functionality. The probing of catalysis on a diamond surface can be accomplished, in principle, by using surface-implanted NV centers to monitor single nuclear spins of the catalyst (see Fig. 1), which yields valuable information about the catalytic reaction, e.g., about conformational changes. As the probing method is label-free it is also suitable for more general biosensing applications [11, 12]. While this prospect is certainly appealing, the important question remains of whether NV-based sensing of nuclear spins is still efficiently achievable under ambient thermal conditions, i.e., when the nuclear target spins exhibit random thermal motion.

In this paper we show that the detection of nuclear spins (and target spins in general) undergoing thermal diffusion is indeed feasible under realistic experimental conditions. We focus our attention on the nuclear spin of

a fluorine atom covalently bound to a ruthenium-based catalyst (NHC-Ru complex [13]) and analyze the time-resolved sensing of a possible detachment of the fluorine from the catalyst. Our theoretical study is strongly motivated by recent experimental progress: Decoupling schemes for the electron spin of the NV now offer the possibility to resonantly amplify interactions between the NV center and selected spin targets and to suppress decoherence caused by surrounding spins. In this way, single nuclear spins located in the diamond lattice are routinely detected by employing either pulsed or continuous dyna-

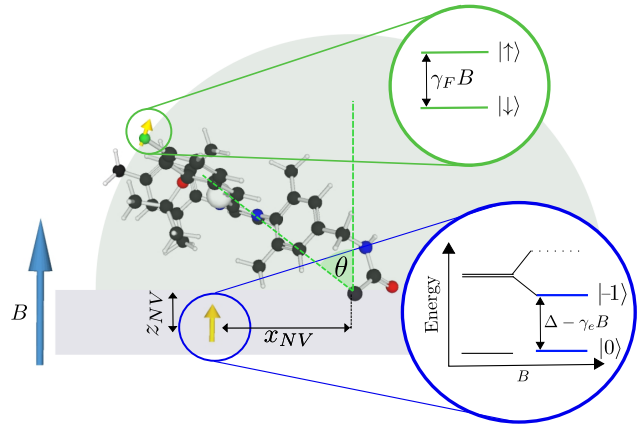


FIG. 1. Sensing of a single fluorine atom undergoing random thermal motion using a single near-surface nitrogen-vacancy center in bulk diamond: The fluorine-containing molecule (N-heterocyclic carbene-ruthenium complex) is covalently attached to the diamond and rotates freely around its anchor point, confining the thermal motion of the fluorine to a spherical surface. The nuclear spin of the fluorine and the microwave-driven electron spin of the NV center interact resonantly at the Hartmann-Hahn matching condition. Time-resolved sensing of the fluorine in thermal motion is achieved by observing the polarization transfer between the spins.

mical decoupling [14–16]. The achieved sensitivity of NV centers has moreover been shown to be sufficient to discern even single spin targets or molecules on the diamond surface [7–9] and also to detect spin ensembles surrounding NV centers hosted in nanodiamonds [17].

To make the analysis more definite we consider continuous dynamical decoupling of the NV center in combination with the Hartmann-Hahn double resonance (HHDR) scheme [18], which has been successfully used for detecting single static target spins [16]. At first we substantially extend the existing theory on the HHDR scheme for NV centers [16, 19] by including the effects caused by the motion of the target spin. Making use of a stochastic description of the diffusive target we derive an effective quantum master equation for the evolution of the spin system formed by the NV center and the target. We find in particular that the evolution of the spin system for a target undergoing fast diffusion is remarkably similar to the case of a static target, but with an effective *averaged* NV-target coupling replacing the static NV-target coupling. Details of the motion of the target are obtained from anisotropic network model (ANM) simulations [20–22] of the entire NHC-Ru complex. The results of the ANM simulation allow us to generate stochastic trajectories of the target spin only, which in turn can be used for estimating the parameters of the effective quantum master equation.

When applied to the fluorine attached to the NHC-Ru complex our approach yields that the effective NV-target coupling can reach values up to a few hundred kilohertz and therefore is sufficiently strong for observable HHDR polarization transfers between the spins to be achieved. The motion of the target spin also results in diffusion-induced decoherence of the NV spin, which is however negligible. As a result, the detachment of a target spin from the NHC-Ru carrier molecule can be monitored with a time resolution of a few seconds. In addition, we analyze an alternative scenario, where an electron spin label is attached to a CXCR4 chemokine receptor, which plays an important role in infection processes [23]. Unlike in the previous application, the NV center used to detect the spin label is inside a nanodiamond that is attached to the same receptor. Our results indicate that spin labels at a distance of 10 nm from the NV center can be monitored with a sub-second time resolution despite the thermal vibrations of the chemokine receptor.

The paper is organized as follows: In Sec. II, a detailed description of the system and the Hartmann-Hahn resonance scheme is presented. In Sec. III we characterize the motion of the NHC-Ru complex by means of ANM simulations and introduce stochastic differential equations for generating stochastic trajectories of the target spin. In Sec. IV we start from the stochastic Hamiltonian of the NV-target system and derive the quantum master equation for the coupled spins. In Sec. V we discuss the feasibility of the spin detection considering the relaxation time of the NV spin and the NV readout photon collection efficiency. In Sec. VI we briefly analyze the detection of an electron spin label on a CXCR4 chemokine receptor

by using a proximate NV center in a nanodiamond. We end with the conclusions in Sec. VII.

II. MODEL AND STOCHASTIC APPROACH

Starting with our main application, we consider a fluorine atom bound to the NHC-Ru molecule, which is covalently attached to the surface of the diamond and rotates freely around its anchor point (see Fig. 1). In general, the carrier molecule can be flexible, but the NHC-Ru complex considered here exhibits only small changes in shape. The NHC-Ru molecule is immersed in a layer of water, deposited uniformly on the surface of the diamond, and undergoes fast diffusive motion due to thermal fluctuations (the environment being at room temperature). The NV center is implanted close to the diamond surface and in the vicinity of (but not necessarily directly underneath) the anchor point. We do not expect to have full control over the positions so that the details of the setup rely on the statistical proximity between the NV center and the molecule. The axis of the NV center is assumed to be perpendicular to the diamond surface for concrete applications in Sec. V.

A. Coupling between NV center and target spin

The NV center and the fluorine atom (i.e. the target spin) are coupled through the magnetic dipole-dipole interaction between their electronic and nuclear spins, respectively. The NV ground state is an electronic spin triplet (spin $S = 1$) with three states having spin projections $|m_s = 0\rangle$ and $|m_s = \pm 1\rangle$ along the NV axis, defining the z -axis of our coordinate system. In what follows, the states $|m_s = 0\rangle$ and $|m_s = \pm 1\rangle$ will be denoted as $|0\rangle$ and $|\pm 1\rangle$, respectively. The target spin is a nuclear spin doublet (spin $S = 1/2$) with spin projections $|\uparrow\rangle$ and $|\downarrow\rangle$. The degeneracy of the states $|-1\rangle$, $|+1\rangle$, both separated from $|0\rangle$ by the zero-field splitting $\Delta = 2.87$ GHz, is lifted by the external magnetic field \mathbf{B} such that a continuous microwave field resonant with the $|0\rangle \leftrightarrow |-1\rangle$ transition can be applied (see Fig. 1). The NV center is then described within the $|0\rangle$, $|-1\rangle$ subspace by the microwave dressed states $|\pm\rangle = (|0\rangle \pm |-1\rangle)/\sqrt{2}$ separated by twice the Rabi frequency Ω [24].

The time-varying Hamiltonian used to describe the coupled spin system in the secular approximation and the dressed state basis is given by [16, 19]

$$H(t) = \Omega\sigma_z^e + \gamma_N \mathbf{B}_{\text{eff}}(t) \cdot \boldsymbol{\sigma}^N - \sigma_x^e [\mathbf{A}(t) \cdot \boldsymbol{\sigma}^N], \quad (1)$$

where $\mathbf{A}(t)$ is the hyperfine vector, $\mathbf{B}_{\text{eff}}(t) = \mathbf{B} - \frac{1}{2}\gamma_N^{-1}\mathbf{A}(t)$ is the effective magnetic field and γ_N is the nuclear gyromagnetic ratio. The spin operators σ_j^e and σ_j^N (with $j = x, y, z$) act on the states $|+\rangle$, $|-\rangle$ and $|\uparrow\rangle$, $|\downarrow\rangle$, respectively. The time dependence of the hyperfine vector $\mathbf{A}(t)$ stems from the fluctuating position of

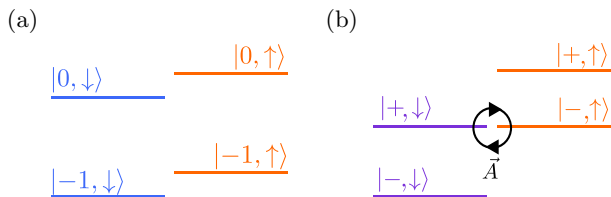


FIG. 2. Energy-level diagram of the electronic spin $|0\rangle, |-1\rangle$ of the NV center and the nuclear spin $|\uparrow\rangle, |\downarrow\rangle$ of the fluorine atom. (a) The mismatch between the electronic and nuclear energy scales suppresses the polarization transfer between the states $|0, \downarrow\rangle$ and $|-1, \uparrow\rangle$ induced by the hyperfine coupling \mathbf{A} . (b) Continuous microwave driving of the electronic states enables polarization transfer between the dressed states $|+, \downarrow\rangle$ and $|-, \uparrow\rangle$ under the Hartmann-Hahn matching condition.

the fluorine $\mathbf{r}(t)$ relative to the NV center. Specifically, $\mathbf{A}(t) \equiv \mathbf{A}[\mathbf{r}(t)]$ and $\mathbf{r}(t)$ are related at every instant of time by

$$\mathbf{A}(\mathbf{r}) = -\frac{\mu_0 \gamma_e \gamma_N}{4\pi |\mathbf{r}|^3} (3\hat{r}_x \hat{r}_z, 3\hat{r}_y \hat{r}_z, 3\hat{r}_z^2 - 1), \quad (2)$$

where \hat{r}_j are the components of the unit vector $\hat{\mathbf{r}} \equiv \mathbf{r}/|\mathbf{r}|$. Moreover, γ_e and γ_N are the electronic and nuclear gyromagnetic ratios, respectively, and μ_0 is the vacuum permeability.

The Hamiltonian in Eq. (1) has been shown to accurately describe the standard HHDR scheme [18], which has been employed in a recent experiment to detect *static* target spins by using a single NV center [16]. Specifically, under the Hartman-Hahn matching condition $\Omega - \gamma_N |\mathbf{B}_{\text{eff}}| = 0$, the states $|+, \downarrow\rangle$ and $|-, \uparrow\rangle$ of the coupled spin system become resonant, which results in coherent polarization transfer between them (see Fig. 2). In the ideal HHDR scheme, the NV spin is first optically pumped into the state $|0\rangle$ and rotated to $|+\rangle$ with a $\pi/2$ microwave pulse. If the target spin is in state $|\downarrow\rangle$ then the system is thus prepared in state $|+, \downarrow\rangle$ and undergoes coherent oscillations between the $|+, \downarrow\rangle$ and $|-, \uparrow\rangle$ states. The polarization transfer resulting in the state $|-, \uparrow\rangle$ after the interrogation time τ_{int} serves as experimental indicator for the presence of the target spin, observed as modulations in the NV fluorescence after mapping the states $|+\rangle, |-\rangle$ back to $|0\rangle, |-1\rangle$ with a second $\pi/2$ pulse. The preparation, polarization transfer and optical read-out of the NV spin are in principle identical for static and diffusive target spins. In practice, however, the transfer is affected by different decoherence mechanisms and the target spin is initially in a mixed state, which will be shown to reduce the observed polarization transfer.

B. Stochastic description of diffusive target spins

When applying the HHDR scheme to the diffusive target spin we face the additional complication that its position $\mathbf{r}(t)$ undergoes random fluctuations, i.e., Brownian motion, as a consequence of the thermal environment.

This motivates our main assumption, namely that the position $\mathbf{r}(t)$ and the hyperfine vector $\mathbf{A}(t)$ are stochastic processes, i.e., random functions of time. As a consequence, the time evolution governed by $H(t)$ becomes a stochastic differential equation.

To make the problem more tractable we restrict ourselves to the case where $\mathbf{r}(t)$ and $\mathbf{A}(t)$ are strictly stationary stochastic processes [25]. This implies that $\mathbf{A}(t)$ has a stationary probability distribution $p_{\mathbf{A}}(\mathbf{s})$ with mean $\mathcal{A} = \langle \mathbf{A}(t) \rangle_{\text{p}}$ and variance $\sigma^2 = \langle (\mathbf{A}(t) - \mathcal{A})^2 \rangle_{\text{p}}$, where $\langle \cdot \rangle_{\text{p}}$ denotes averaging with respect to $p_{\mathbf{A}}(\mathbf{s})$. We further assume that $\mathbf{A}(t)$ is fully specified by the two-point correlations $C_{ij}(\tau) \equiv \langle \xi_i(t+\tau) \xi_j(t) \rangle_{\text{tr}}$ expressed in terms of the fluctuations of the hyperfine vector $\xi_j(t) = A_j(t) - \mathcal{A}_j$, where now the average $\langle \cdot \rangle_{\text{tr}}$ is taken over all diffusive trajectories of the target spin. Instead of using correlations $C_{ij}(\tau)$ we can characterize $\xi(t)$ in an equivalent way by the power spectra

$$S_{ij}(\omega) = \int_{-\infty}^{\infty} d\tau C_{ij}(\tau) e^{-i\omega\tau}. \quad (3)$$

For the common case of exponentially decaying correlations $C_{ij}(\tau) = \sigma_{ij}^2 e^{-|\tau|/\tau_{ij}}$ the power spectra are $S_{ij}(\omega) = 2\sigma_{ij}^2 \tau_{ij} / (1 + \omega^2 \tau_{ij}^2)$, where σ_{ij}^2 are the amplitudes of the fluctuations and τ_{ij} the correlation times.

Our general approach is to divide the task of determining the evolution of the coupled spin system into two independent parts: The first part deals with the characterization of the diffusive motion of the target spin in terms of the distribution $p_{\mathbf{A}}(\mathbf{s})$ and the correlations $C_{ij}(\tau)$. The second part consists of solving, at least approximately, the evolution of the spin system according to $H(t)$ with the distribution $p_{\mathbf{A}}(\mathbf{s})$ and the power spectra $S_{ij}(\omega)$ as given ingredients.

III. DIFFUSION OF THE TARGET SPIN

To efficiently characterize the diffusive motion of the molecule and the fluorine on different time scales we use short-time ANM simulations in combination with an effective description based on stochastic trajectories. More precisely, ANM simulations are used to simulate the dynamics of the entire carrier molecule, whereas stochastic trajectories provide a simple but still accurate description of the random motion of the fluorine or the target spin in general. The time τ_{exp} required for the fluorine to explore the available spatial domain (see Fig. 3) roughly defines the time scale separating the two descriptions.

A. Anisotropic network model simulations

Numerical simulations allow us to obtain physically accurate details of the motion of the carrier molecule to which the target spin is bound, either the NHC-Ru complex or the chemokine receptor. Apart from ANM simulations, several alternative numerical methods have been

proposed to predict molecular motion, including molecular dynamics (MD) [26, 27] and normal mode analysis (NMA) [28]. ANM simulations are particularly suitable for our purposes for the following two reasons: Considering the large disparity in time scales between the molecular motion and spin evolution we are interested only in the slowest molecular degrees of freedom, i.e., rotations and low-frequency vibrations, which have been shown to be accurately reproduced by the ANM. Moreover, ANM simulations are computationally less costly than fully microscopic MD simulations and therefore applicable to biologically relevant molecules of considerable size.

In essence, the ANM is a coarse-grained description of the collective dynamics of the molecule, independent of the atomic details [20–22]. Regardless of specific atomic interactions, all atoms within a chosen cutoff distance R_c interact via pairwise harmonic potentials whose strength is characterized by a phenomenological spring constant κ , assumed to be the same for all atom pairs [20]. The values of R_c and κ are obtained by comparing ANM results to MD simulations and experimental data [21], where larger cutoffs R_c (implying more interacting pairs) can be compensated by smaller spring constants κ [22]. The only remaining parameters entering the simulation are the equilibrium positions of the atoms forming the molecule, depicted in Fig. 1 for the NHC-Ru complex. The collisions of the molecule with the constituents of the solvent at ambient temperature are mimicked by augmenting the ANM simulations with a Langevin dynamics, i.e., damped random kicks, for each atom of the molecule [29]. In this way, we have complete access to the trajectories of the target spin, which depend on the shape and stiffness of the molecule, the solvent and its temperature [30–32].

When applied to the NHC-Ru molecule we use the values for the spring constant $\kappa = 1 \text{ kcal}/(\text{mol } \text{Å}^2)$, the cutoff distance $R_c = 10 \text{ Å}$, the damping coefficient of the Langevin dynamics $\zeta = 5 \text{ ps}^{-1}$ and the solvent temperature $T = 300 \text{ K}$. The ANM simulations with this set of parameters have been tested against MD simulations and are expected to give reliable results for the rotations of the NHC-Ru complex and the low-frequency vibrations of CXCR4 chemokine receptor. The molecular geometry and the atomic numbers of the constituents of the NHC-Ru complex are provided in XYZ file format as Supplemental Material [33].

Figure 3 shows representative sample trajectories of the fluorine atom attached to the NHC-Ru complex on the time scale of microseconds. The fluorine undergoes a diffusive motion within a narrow spherical shell whose thickness is determined by small oscillations of the NHC-Ru molecule. The motion is restricted to a spherical zone as a result of the presence of the diamond surface and the spatial extent of the molecule. If we neglect the thickness of the shell then the position of the fluorine is conveniently described in a spherical coordinate system centered at the anchor point of the molecule, with azimuthal angle $\varphi \in [0, 2\pi]$ and polar angle $\theta \in [0, \pi/2]$. Within this parametrization, we extract the properties

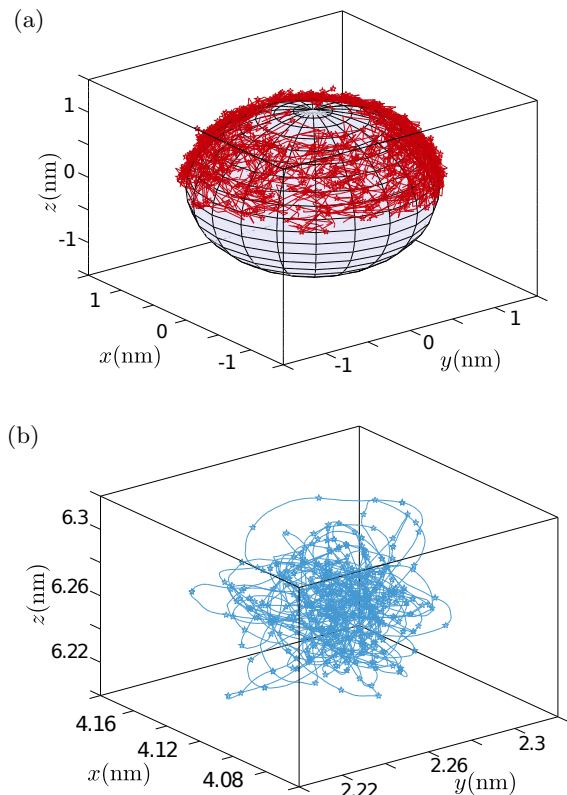


FIG. 3. Trajectories of the target spin obtained from short-time ANM simulations. (a) The fluorine atom bound to the NHC-Ru molecule follows a stochastic trajectory on a spherical surface. (b) The spin label attached to the chemokine receptor CXCR4 exhibits damped fluctuations around its equilibrium position with respect to the NV center.

of the diffusive motion in the form of the distributions $p_\theta(s)$ and $p_\varphi(s)$ of the polar and azimuthal angle, respectively, and the rotational diffusion coefficient \mathcal{D}_r , as shown in Fig. 4. In particular, the mean square displacement $\langle \Delta\theta^2(t) \rangle_{\text{tr}}$ in the regime $t \ll \tau_{\text{exp}}$ allows us to determine the diffusion coefficient \mathcal{D}_r from the short-time relation $\langle \Delta\theta^2(t) \rangle_{\text{tr}} = 2\mathcal{D}_r t$. The value of the diffusion coefficient extracted from ANM simulations is $\mathcal{D}_r = 2.1 \text{ ns}^{-1}$ for the specific NHC-Ru molecule immersed in water at room temperature.

We can also estimate the diffusion coefficient \mathcal{D}_r by resorting to semi-empirical formulas, either as a practical alternative to ANM simulations or to gain some intuition about the molecular motion. If the approximately rod-shaped NHC-Ru molecule is modeled as a cylinder of length L and diameter d and the attachment to the diamond surface is neglected then the rotational diffusion coefficient may be obtained from [30]

$$\mathcal{D}_r = \frac{3k_B T}{\pi\eta L^3} [\log p + c(p)], \quad (4)$$

with $c(p) = -0.05/p^2 + 0.917/p - 0.662$. The diffusion coefficient \mathcal{D}_r depends on the ratio $p = L/d$, the Boltzmann factor $k_B T$ and the viscosity of the solvent η . The

coefficient \mathcal{D}_r depends crucially on the length L , implying that larger molecules undergo slower diffusion. For a molecule of size $L = 1.5$ nm and $d = 1.1$ nm dissolved in water at $T = 300$ K with viscosity $\eta = 10^{-3}$ Pa s we obtain $\mathcal{D}_r = 0.3$ ns $^{-1}$, thereby underestimating the more accurate simulation result.

B. Stochastic trajectories and correlation functions

In order to specify the correlations $C_{ij}(\tau)$ we require stochastic trajectories on longer time scales than accessible by numerically costly ANM simulations. For that purpose we generate stochastic trajectories of the fluorine on a spherical surface using the stochastic differential equations in Itô form [34]:

$$\begin{aligned} d\theta(t) &= \frac{\mathcal{D}_r}{\tan \theta(t)} dt + \sqrt{2\mathcal{D}_r} dW_1(t) \\ d\varphi(t) &= \frac{\sqrt{2\mathcal{D}_r}}{\sin \theta(t)} dW_2(t), \end{aligned} \quad (5)$$

where $dW_1(t)$ and $dW_2(t)$ are two independent Wiener processes and dt is the time differential. In this setting, we neglect the spatial extent of the molecule and restrict the motion of the fluorine to a spherical zone limited by the polar angles θ_{\min} and θ_{\max} , which is implemented through reflective boundary conditions for Eqs. (5). The distribution of the fluorine on the spherical zone resulting from Eqs. (5) is uniform; the corresponding distributions of the angles are $p_\varphi(s) = 1/2\pi$, with $s \in [0, 2\pi]$, and

$$p_\theta(s) = \frac{\sin(s)}{\cos(\theta_{\min}) - \cos(\theta_{\max})}, \quad (6)$$

with $s \in [\theta_{\min}, \theta_{\max}]$. The angles θ_{\min} and θ_{\max} are chosen to best fit the ANM results for $p_\theta(s)$, as illustrated in Fig. 4(b). However, the results of our analysis are rather robust with respect to the choice of θ_{\min} and θ_{\max} , which alternatively may be estimated based on the shape of the molecule.

Now, for a generic stochastic process $u(t)$ evolving according to $du(t) = a[u(t)]dt + b[u(t)]dW(t)$, with drift coefficient $a[u(t)]$ and diffusion coefficient $b[u(t)]$, one obtains numerically generated trajectories by using the corresponding finite difference equation

$$u(t + \delta t) = u(t) + a[u(t)]\delta t + b[u(t)](\delta t)^{1/2}N(t), \quad (7)$$

where δt is the discrete time step and $N(t)$ is a temporally uncorrelated normal random variable, i.e., $N(t)$ is statistically independent of $N(t')$. We apply the finite difference approach to generate trajectories $[\theta(t), \varphi(t)]$ based on Eqs. (5) with the parameters θ_{\min} , θ_{\max} and \mathcal{D}_r obtained from ANM simulations. Trajectories of the position $\mathbf{r}(t)$ relative to the NV center and the hyperfine vector $\mathbf{A}(t)$ are then readily found from $[\theta(t), \varphi(t)]$.

The two-point correlations $C_{ij}(\tau)$ (with $i, j = x, y, z$) obtained from Monte Carlo sampling over trajectories are

shown in Fig. 5. While the details of $C_{ij}(\tau)$ depend on the random positioning of the NV center, we find that the correlations decay quickly with time. This ensures that the power spectra $S_{ij}(\omega)$ and integrals over the two-point correlations $C_{ij}(\tau)$ are well defined, and that the Markov approximation is applicable in Sec. IV B. In fact, the specific dependence of the stochastic equations (5) on the diffusion coefficient \mathcal{D}_r implies that all correlation functions $C_{ij}(\tau)$ decay on a time scale set by \mathcal{D}_r^{-1} and thus $\tau_{ij} \sim \mathcal{D}_r^{-1}$ for exponentially decaying $C_{ij}(\tau)$ (see the Appendix for details).

IV. EVOLUTION OF THE COUPLED SPINS

For the analysis of the stochastic evolution we split the Hamiltonian $H(t)$ into a time-independent average Hamiltonian $H_A = \langle H(t) \rangle_p$ and the remaining stochastic part $H_\xi(t) = H(t) - \langle H(t) \rangle_p$, which read as

$$\begin{aligned} H_A &= \Omega \sigma_z^e + \left(\gamma_N \mathbf{B} - \frac{1}{2} \mathbf{A} \right) \cdot \boldsymbol{\sigma}^N - \sigma_x^e [\mathbf{A} \cdot \boldsymbol{\sigma}^N] \\ H_\xi(t) &= -\frac{1}{2} \boldsymbol{\xi}(t) \cdot \boldsymbol{\sigma}^N - \sigma_x^e [\boldsymbol{\xi}(t) \cdot \boldsymbol{\sigma}^N]. \end{aligned} \quad (8)$$

We note that H_A is identical to the Hamiltonian for a static target spin, where the constant hyperfine vector \mathbf{A} is replaced by the mean $\mathbf{A} = \langle \mathbf{A}(t) \rangle_p$, while $H_\xi(t)$ depends only on the fluctuations $\boldsymbol{\xi}(t)$ of the hyperfine vector. The evolution of the density matrix $\rho(t)$ of the spin system is governed by the Liouville equation

$$\frac{\partial}{\partial t} \rho(t) = [\mathcal{L}_A + \mathcal{L}_\xi(t)] \rho(t) \quad (9)$$

where the Liouvillian operators are defined as $\mathcal{L}_A = -i[H_A, \cdot]$ and $\mathcal{L}_\xi(t) = -i[H_\xi(t), \cdot]$. As it stands, Eq. (9) describes the evolution of the coupled spins for a single diffusive trajectory of the target spin, encoded in the fluctuations $\boldsymbol{\xi}(t)$. Since we can control neither the initial position nor the trajectories of the target spin our goal is to determine $\langle \rho(t) \rangle_{\text{tr}}$, i.e., the density matrix $\rho(t)$ averaged over all possible trajectories $\boldsymbol{\xi}(t)$ with random initial conditions.

A straightforward way to calculate $\langle \rho(t) \rangle_{\text{tr}}$ approximately is by Monte Carlo sampling: For a representative ensemble of trajectories $\{\boldsymbol{\xi}(t)\}$ one solves Eq. (9) numerically for each $\boldsymbol{\xi}(t)$ and takes the ensemble average of the resulting density matrices to obtain $\langle \rho(t) \rangle_{\text{tr}}$. The trajectories $\boldsymbol{\xi}(t)$ may be generated by following the procedure outlined in Sec. III B. We will use Monte Carlo sampling to confirm and complement our analytical results at the end of this section.

Approximate analytical descriptions for the evolution of $\langle \rho(t) \rangle_{\text{tr}}$ can be obtained for several relevant parameter regimes of the system. The starting point is the stochastic Liouville equation [25, 35]

$$\begin{aligned} \frac{\partial}{\partial t} \langle \rho(t) \rangle_{\text{tr}} &= \mathcal{L}_A \langle \rho(t) \rangle_{\text{tr}} \\ &+ \int_0^t d\tau \langle \mathcal{L}_\xi(t) e^{\mathcal{L}_A \tau} \mathcal{L}_\xi(t - \tau) \rangle_{\text{tr}} e^{-\mathcal{L}_A \tau} \langle \rho(t) \rangle_{\text{tr}}, \end{aligned} \quad (10)$$

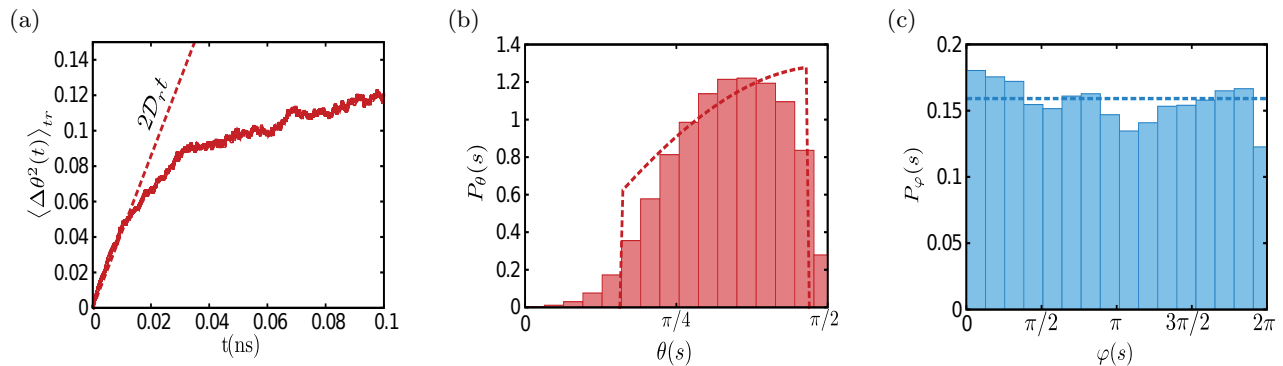


FIG. 4. The properties of the diffusive motion of the fluorine (target spin) extracted from the ANM simulations. (a) The mean square displacement $\langle \Delta\theta^2(t) \rangle_{\text{tr}}$ as a function of time t yields the diffusion coefficient $\mathcal{D}_r = 2.1 \text{ ns}^{-1}$ from the short-time relation $\langle \Delta\theta^2(t) \rangle_{\text{tr}} = 2\mathcal{D}_r t$. The histograms (b) and (c) show the distributions $p_\theta(s)$ and $p_\varphi(s)$ of the polar and azimuthal angle, respectively. The dotted lines in (b) and (c) indicate $p_\varphi(s)$ and $p_\theta(s)$ expected from a uniform distribution of the fluorine on a spherical zone limited by the polar angles θ_{\min} and θ_{\max} .

which is obtained by formally integrating the Liouville equation (9) and performing a cumulant expansion up to second order in $\mathcal{L}_\xi(t)$. The applicability of Eq. (10) is limited by the amplitude of the fluctuations $\xi(t)$ and their correlation times, which can be quantified by the typical amplitude and width of $C_{ij}(\tau)$, denoted by $\hat{\sigma}^2$ and $\hat{\tau}$, respectively. The cumulant expansion includes terms up to order $\hat{\sigma}^2 \hat{\tau} t$, which implies that Eq. (10) is valid under the condition $\hat{\sigma}^2 \hat{\tau} \ll \tau_{\text{int}}^{-1}$ for spin evolutions up to the interrogation time τ_{int} .

We now discuss three different regimes for which analytical approximations are obtained: the fast-diffusion regime with $\hat{\tau} \rightarrow 0$ and arbitrarily large $\hat{\sigma}^2$, the moderate-diffusion regime with finite $\hat{\sigma}^2$ and $\hat{\tau}$, and the slow-diffusion regime with $\hat{\tau} \gg \tau_{\text{int}}$.

A. Fast-diffusion regime

For vanishingly small correlation times $\hat{\tau} \rightarrow 0$ the second order term in Eq. (10) and higher order terms of the cumulant expansion vanish. The evolution of the spin system is governed solely by the average Hamiltonian H_A in Eq. (8). The only difference from a static target spin is that the hyperfine vector \mathbf{A} is replaced by the mean \mathcal{A} of the stationary process $\mathbf{A}(t)$ over the distribution $p_A(\mathbf{s})$. This simplifies the description of the system considerably because no averaging over trajectories is required.

Analogously to the static case [16, 19] we determine the dynamics of the spins according to H_A (with the magnetic field \mathbf{B} along the NV axis). In the vicinity of the Hartmann-Hahn matching condition, i.e., close to vanishing averaged detuning $\delta = \frac{1}{2}(\Omega - \gamma_N B_z + \frac{1}{2}\mathcal{A}_z)$, transitions to the off-resonant states $|+, \uparrow\rangle$ and $|-, \downarrow\rangle$ are suppressed by the factor $(\mathcal{A}/\Omega)^2$ of the order 10^{-5} . This allows us to reduce the system to the two-dimensional subspace $|+, \downarrow\rangle, |-, \uparrow\rangle$ with the corresponding Hamiltonian

$$\tilde{H}_A = 2\delta\tilde{\sigma}_z - \frac{1}{2}\mathcal{A}_x\tilde{\sigma}_x + \frac{1}{2}\mathcal{A}_y\tilde{\sigma}_y, \quad (11)$$

where the Pauli matrices $\tilde{\sigma}_j$ act on the subspace only. For the nuclear spin of the fluorine in a completely mixed state and the NV center initially in the state $|+\rangle$, we then obtain the probability $P(t, \delta)$ of finding the NV center in the reversed state $|-\rangle$ after the time t

$$P(t, \delta) = \frac{1}{2} \frac{\mathcal{J}^2}{\mathcal{J}^2 + \delta^2} \sin^2(\sqrt{\mathcal{J}^2 + \delta^2} t), \quad (12)$$

where we introduced the averaged coupling between the NV and the target spin $\mathcal{J} = \frac{1}{4}(\mathcal{A}_x^2 + \mathcal{A}_y^2)^{1/2}$. The maximal polarization transfer occurs at resonance $\delta = 0$ after a time $t = \pi/2\mathcal{J}$, which implies that the interrogation time τ_{int} is of the order of $1/\mathcal{J}$, typically in the millisecond regime (see also Sec. V).

B. Moderate-diffusion regime

In the moderate-diffusion regime with a finite correlation time $\hat{\tau}$, one has to take the second order correction in Eq. (10) into account. However, since the evolution according to H_A is slow on a time scale set by $\hat{\tau}$, i.e., $\mathcal{J}\hat{\tau} \ll 1$, we can neglect the exponentials $e^{\pm\mathcal{L}_A\tau}$ and obtain

$$\frac{\partial}{\partial t} \langle \rho(t) \rangle_{\text{tr}} = \left(\mathcal{L}_A + \int_0^t d\tau \langle \mathcal{L}_\xi(t) \mathcal{L}_\xi(t-\tau) \rangle_{\text{tr}} \right) \langle \rho(t) \rangle_{\text{tr}}. \quad (13)$$

The effect of the stochastic part is best understood when Eq. (13) is reduced to a Markovian master equation in Lindblad form [36, 37]. In the Markov approximation we extend the upper limit of the integral in Eq. (13) to infinity and introduce the rates $\gamma_{ij} = S_{ij}(\omega = 0)$, which for the particular case of exponentially decaying correlations $C_{ij}(\tau) = \sigma_{ij}^2 e^{-|\tau|/\tau_{ij}}$ are given by $\gamma_{ij} = 2\sigma_{ij}^2 \tau_{ij}$. More generally, we note that the matrix Γ constituted by the elements γ_{ij} is positive definite for any form of the correlations $C_{ij}(\tau)$ [38]. After a change to the eigenbasis of the symmetric matrix Γ , having eigenvalues γ_k , the

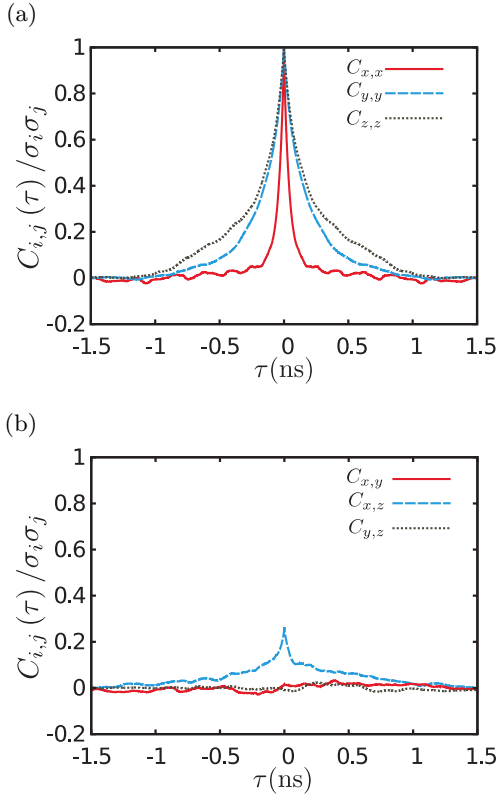


FIG. 5. Characterization of the thermal fluctuations $\xi(t)$ of the hyperfine vector. The correlations $C_{ij}(\tau)$ are normalized by the standard deviations σ_i of the fluctuations. (a) The autocorrelations $C_{ii}(\tau)$ are, to a good approximation, exponential decay curves with a typical correlation time of $\tau_{ij} \sim 0.1$ ns. (b) The cross-correlations $C_{ij}(\tau)$ with $i \neq j$ are found to be significantly smaller than the autocorrelations.

resulting Lindblad equation reads as

$$\frac{\partial}{\partial t} \langle \rho(t) \rangle_{\text{tr}} = -i[H_A, \langle \rho(t) \rangle_{\text{tr}}] + \mathcal{L}_{\text{diff}} \langle \rho(t) \rangle_{\text{tr}} \quad (14)$$

with the diffusion-induced dissipative part

$$\mathcal{L}_{\text{diff}} \langle \rho(t) \rangle_{\text{tr}} = \sum_k \frac{\gamma_k}{2} \left(L_k \langle \rho(t) \rangle_{\text{tr}} L_k^\dagger - \frac{1}{2} \{ L_k^\dagger L_k, \langle \rho(t) \rangle_{\text{tr}} \} \right), \quad (15)$$

where $\{, \}$ stands here for the anticommutator. The three Lindblad operators in Eq. (15) acting on both spins are given by $L_k = L_k^\dagger = \check{\sigma}_k^N \otimes (\sigma_x^e + \frac{1}{2}\mathbb{1})$, where $\check{\sigma}_k^N$ are the Pauli matrices along the axes defined by the eigenbasis of Γ . This effective description of the coupled spin system in the form of Eqs. (14) and (15) greatly simplifies the analysis of the HHDR scheme and is applicable for a large range of the detuning δ .

It can be seen from Eq. (14) that the coherent evolution is determined by the averaged Hamiltonian H_A , as in the fast-diffusion regime, while the diffusion-induced dissipative part of Eq. (14) has two effects: The operators $\check{\sigma}_k^N$ act in three spatial directions on the nuclear spin and result in its depolarization. The operator σ_x^e acting on the NV center causes spin flips between $|+\rangle$ and

$|-\rangle$, which directly affect the Hartmann-Hahn polarization transfer. In fact, the dissipative part results from averaging over dissimilar trajectories $\xi(t)$, which during the interrogation time τ_{int} explore slightly different domains accessible to the hyperfine vector. This is a consequence of the finite correlations in combination with the random initial values of $\xi(t)$. On the other hand, the polarization transfer when only a single diffusive trajectory of the fluorine is considered remains always coherent.

C. Slow-diffusion regime

In the slow-diffusion regime we assume that the hyperfine vector $\mathbf{A}(t)$ is constant during the interrogation time τ_{int} , but drifts slowly during repeated measurements of the Hartmann-Hahn polarization transfer. This means that $\tau_{\text{int}} \ll \hat{\tau} \ll N\tau_{\text{int}}$, where N is the number of individual measurement runs that are performed. This regime was also analyzed in the context of magnetometry with rotationally diffusing nanodiamonds [39].

To obtain the averaged density matrix $\langle \rho(t) \rangle_{\text{tr}}$ we determine the spin dynamics according to the time-independent Hamiltonian H as for the static case, but with the hyperfine vector \mathbf{A} as a random variable with distribution $p_{\mathbf{A}}(\mathbf{s})$. This yields the density matrix $\rho(t, \mathbf{A})$ for each \mathbf{A} , from which we obtain

$$\langle \rho(t) \rangle_{\text{tr}} = \int d\mathbf{s} p_{\mathbf{A}}(\mathbf{s}) \rho(t, \mathbf{s}). \quad (16)$$

The density matrix $\langle \rho(t) \rangle_{\text{tr}}$ is expected to accurately describe the observed experimental results in the limit of large N .

To emphasize the difference from the fast-diffusion regime we give the explicit expression for the probability $P(t, \delta)$ of the transition from state $|+\rangle$ to $|-\rangle$. According to the prescription in Eq. (16) this probability is given by

$$P(t, \Omega) = \frac{1}{2} \int d\mathbf{s} p_{\mathbf{A}}(\mathbf{s}) \frac{J^2(\mathbf{s})}{J^2(\mathbf{s}) + \delta^2(\mathbf{s})} \sin^2 [\nu(\mathbf{s}) t], \quad (17)$$

where the detuning $\tilde{\delta}(\mathbf{A}) = \frac{1}{2}(\Omega - \gamma_N B_z + \frac{1}{2}A_z)$, the coupling $J(\mathbf{A}) = \frac{1}{4}(A_x^2 + A_y^2)^{1/2}$ and the effective Rabi frequency $\nu(\mathbf{A}) = [J^2(\mathbf{A}) + \tilde{\delta}^2(\mathbf{A})]^{1/2}$ are random variables. In the slow-diffusion regime we thus solve the equation of motion and subsequently average the solution over $p_{\mathbf{A}}(\mathbf{s})$, in contrast to the fast- and moderate-diffusion regimes, where the equation of motion is solved for averaged detuning δ and coupling \mathcal{J} .

Figure 6 shows the polarization transfer probabilities $P(\tau_{\text{int}}, \Omega)$ for the different diffusion regimes. The general agreement between the analytical results and Monte Carlo sampling over trajectories is illustrated in Figs. 6(a) and 6(b) for a set of generic parameters. The analytical results in Fig. 6(a) are accurate in the regime $\tau_{\text{int}} \ll 1$ ms, as expected from the condition $\delta^2 \hat{\tau} \ll \tau_{\text{int}}^{-1}$

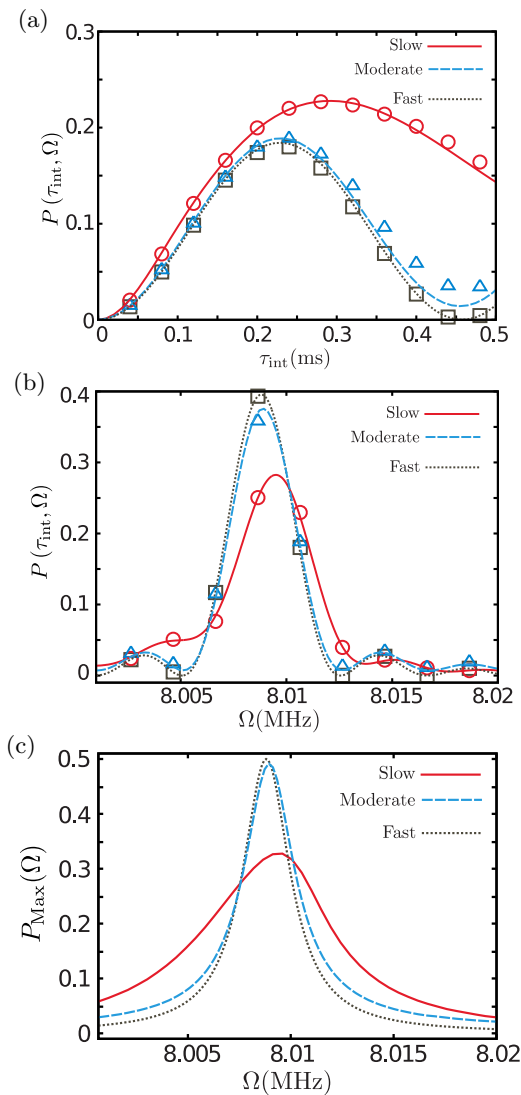


FIG. 6. Polarization transfer probabilities $P(\tau_{\text{int}}, \Omega)$ in the fast-, moderate- and slow-diffusion regimes, obtained from Monte Carlo simulations (symbols) and analytical results (lines). (a) Transfer probability $P(\tau_{\text{int}}, \Omega)$ for fixed Rabi frequency Ω corresponding to a detuning $\delta = 1.8$ kHz. Analytical results and Monte Carlo sampling over trajectories are expected to agree in the regime $\tau_{\text{int}} \ll 1$ ms. (b) Transfer probability $P(\tau_{\text{int}}, \Omega)$ for a fixed interrogation time $\tau_{\text{int}} = 0.25$ ms. (c) Maximum achievable transfer probability $P_{\text{Max}}(\Omega)$ for given Rabi frequency Ω and optimized interrogation time τ_{int} . Perfect polarization transfer $P_{\text{Max}}(\Omega) = 0.5$ is achieved for fast diffusion, while moderate and slow diffusion result in reduced transfer. $\mathcal{D}_r = (0, 10, 10^3) \mu\text{s}^{-1}$ in (a), (b) for the slow-, moderate- and fast-diffusion regimes, and $\mathcal{D}_r = (0, 1, 10^3) \mu\text{s}^{-1}$ in (c), with random initial positions of the target spin.

for the validity of the second order cumulant expansion. The comparison in Fig. 6(b) demonstrates that the analytical approximations are valid even far from resonance. Finally, the maximum achievable transfer probability $P_{\text{Max}}(\Omega)$ for a given Ω and optimized interrogation times τ_{int} is shown in Fig. 6(c). Maximal polarization

transfer is achieved in the fast-diffusion regime, whereas reduced polarization occurs in the moderate- and slow-diffusion regimes due to diffusion-induced decoherence of the NV spin. The most detrimental effect is observed for slow diffusion, where the time scale of the diffusion \mathcal{D}_r^{-1} and the interrogation time τ_{int} are comparable. Note that the resonance of $P_{\text{Max}}(\Omega)$ for fast diffusion (and to a good approximation for moderate diffusion) corresponds to a Lorentzian of width \mathcal{J} centered at $\delta = 0$, whereas the resonance in the slow-diffusion regime is asymmetric and not related to the averaged detuning δ .

V. DETECTION OF FLUORINE DETACHMENT FROM THE MOLECULE

The general formalism developed in the previous section is now applied to the concrete problem of detecting the *detachment* of the fluorine atom from the carrier molecule, which demonstrates the time-resolved operation of the HHDR scheme in a thermal environment. The situation that we envisage here is that the fluorine-marked NHC-Ru complex serves as a catalyst for a chemical reaction. The departure of the fluorine then indicates the event of a chemical reaction that led to the exchange of the fluorine.

As previously shown, the diffusive motion of the fluorine attached to the molecule (in a solvent at room temperature) exhibits short correlation times and the Hartmann-Hahn polarization transfer therefore falls into the fast-diffusion regime, which is accurately described by the corresponding Hamiltonian in Eq. (11). Nevertheless, in order to present the most general situation we take the small diffusion-induced decoherence into account and accordingly extend the analysis to the moderate-diffusion regime. In addition, we include incoherent processes caused by spin flips between the states $|+\rangle$ and $|-\rangle$, which are the main source of decoherence for shallowly implanted NV centers [40]. The effect of spin flips is described by the additional Lindblad dissipator

$$\mathcal{L}_{\text{flip}}\langle\rho(t)\rangle_{\text{tr}} = \frac{\gamma_{\text{flip}}}{2} \sum_j \left(L_j \langle\rho(t)\rangle_{\text{tr}} L_j^\dagger - \frac{1}{2} \{L_j^\dagger L_j, \langle\rho(t)\rangle_{\text{tr}}\} \right),$$

with the Lindblad operators $L_1 = \sigma_+^e$ and $L_2 = \sigma_-^e$, which induce spin flips between the states $|-\rangle$ and $|+\rangle$. The flip rate $\gamma_{\text{flip}} = 1/T_{1\rho}$ is determined by the relaxation time $T_{1\rho}$ in the rotating frame [41], being in the millisecond regime for realistic experimental conditions [40, 42]. The evolution of the spin system is thus governed by the Lindblad equation

$$\frac{\partial}{\partial t} \langle\rho(t)\rangle_{\text{tr}} = -i[H_{\mathcal{A}}, \langle\rho(t)\rangle_{\text{tr}}] + \mathcal{L}_{\text{diff}}\langle\rho(t)\rangle_{\text{tr}} + \mathcal{L}_{\text{flip}}\langle\rho(t)\rangle_{\text{tr}}. \quad (18)$$

We note that the detrimental effect of spin flips on the polarization transfer is significantly stronger than the diffusion-induced decoherence given that $\gamma_{\text{flip}} \gg \gamma_k$. We also recall that the initial state of the fluorine spin is completely mixed, i.e., $\rho(t=0) = |+\rangle\langle+| \otimes \frac{1}{2}\mathbb{I}$, which reduces

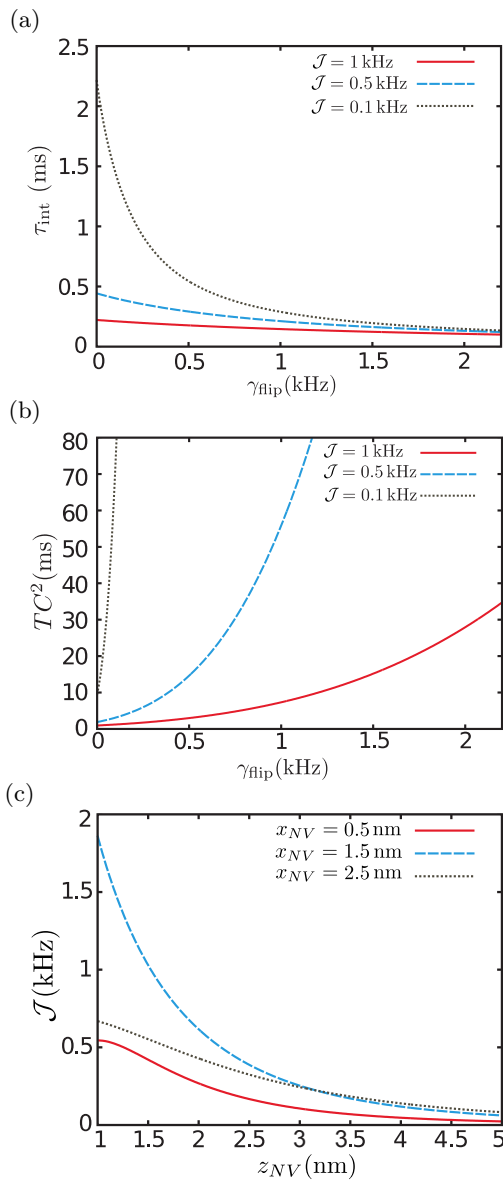


FIG. 7. The time-resolved detection (with unit signal-to-noise ratio) of the detachment of the fluorine from the NHC-Ru carrier molecule. (a) The optimal interrogation time τ_{int} for each measurement run depending on the flip rate γ_{flip} for different couplings \mathcal{J} . With increasing γ_{flip} more runs with shorter interrogation times τ_{int} are required. (b) The overall measurement time T required to detect the detachment as a function of the flip rate γ_{flip} for different couplings \mathcal{J} . (c) The dependence of averaged coupling \mathcal{J} on the depth z_{NV} of the NV center for different lateral offsets x_{NV} with respect to the anchor point of the NHC-Ru molecule (see Fig. 1).

the observable polarization transfer by approximately a factor of two.

The time-resolved detection based on the HHDR scheme is implemented as follows: As long as the fluorine is bound to the molecule the probability of finding the NV center in state $|-\rangle$ after the interrogation time τ_{int} is $P(\tau_{\text{int}}, \delta)$. After the detachment the fluorine dif-

fuses away very rapidly from the molecule due to its small mass so that effectively $\mathcal{J} = 0$ with the corresponding probability $P_{\mathcal{J}=0}(\tau_{\text{int}}, \delta)$. The measurable signal is thus $\Delta P \equiv P(\tau_{\text{int}}, \delta) - P_{\mathcal{J}=0}(\tau_{\text{int}}, \delta)$. The presence of the fluorine is confirmed once the signal-to-noise ratio (R_{SN}) exceeds unity, which for the optical readout of the NV is equivalent to [43]

$$\Delta P \geq \frac{1}{C\sqrt{N}}, \quad (19)$$

where N is the total number of measurements and C specifies the signal contrast and photon collection efficiency.

The optimal time resolution is reached by tuning the interrogation time τ_{int} in dependence on the system parameters, in particular the flip rate γ_{flip} . Since the number of measurements is related to the overall measurement time T through $N = T/(\tau_{\text{int}} + \tau_0)$, with $\tau_0 \ll \tau_{\text{int}}$ the preparation and readout time, we obtain

$$T = \frac{\tau_{\text{int}} + \tau_0}{C^2 \Delta P^2}, \quad (20)$$

from the condition $R_{\text{SN}} = 1$. The main limitation to the time resolution clearly stems from the factor C and the flip rate γ_{flip} (see Table I).

Figure 7 shows the measurement time T and the interrogation time τ_{int} as a function of the flip rate γ_{flip} , as determined from Eq. (18). The detachment of the fluorine can be detected (with unit signal-to-noise ratio) with a time resolution of the order of 10 s under realistic experimental conditions. The general strategy for minimizing the overall measurement time T in the presence of spin flips at rate γ_{flip} is to shorten the interrogation time τ_{int} while increasing the number N of measurement runs. More precisely, the interrogation time τ_{int} scales as $1/\gamma_{\text{flip}}$ as would be expected from a more generic analysis [44].

It can be seen from Fig. 7(b) that short measurement times T require sufficiently strong couplings \mathcal{J} between the NV and the fluorine spin, which in turn are determined by the depth z_{NV} of the NV center and its lateral

z_{NV}	x_{NV}	\mathcal{J}	C^*	$\gamma_{\text{flip}}^\dagger$	τ_{int}	T
2.0 nm	1.5 nm	0.7 kHz	0.05	0.5 kHz	0.23 ms	2.6 s
2.0 nm	1.5 nm	0.7 kHz	0.05	1.0 kHz	0.18 ms	7.9 s
2.0 nm	1.5 nm	0.7 kHz	0.05	2.0 kHz	0.12 ms	37 s
3.0 nm	1.5 nm	0.25 kHz	0.05	0.5 kHz	0.42 ms	45 s
3.0 nm	1.5 nm	0.25 kHz	0.05	1.0 kHz	0.26 ms	250 s

* from Refs. [16, 43]

† from Ref. [40]

TABLE I. Specific values of the model parameters and measurement times T for detecting the fluorine detachment from the NHC-Ru molecule. The coordinates z_{NV} and x_{NV} determine respectively the depth and lateral offset of the NV with respect to the anchor point of the molecule (see Fig. 1). The gyromagnetic ratio of fluorine is $\gamma_{\text{F}} = 40.1 \text{ MHz T}^{-1}$ and the preparation and readout time $\tau_0 \sim 100 \text{ ns}$ is neglected.

offset x_{NV} with respect to the NHC-Ru molecule (see Fig. 1). As shown in Fig. 7(c), the coupling \mathcal{J} decreases monotonically with the depth z_{NV} , where in particular an experimentally accessible depth of $z_{\text{NV}} = 2$ nm corresponds to $\mathcal{J} = 0.7$ kHz for $x_{\text{NV}} = 0.5$ nm. The dependence of \mathcal{J} on the lateral offset x_{NV} with respect to the anchor point of the molecule is characterized by the directionality of the dipolar spin interaction. Qualitatively speaking, the coupling \mathcal{J} is strong if the averaged position of the target spin is located within the dipolar lobes of the NV spin, whereas \mathcal{J} vanishes for the perfectly symmetric configuration $x_{\text{NV}} = 0$ and for large lateral offsets. We finally note that for a fully coherent evolution of the spins ($\gamma_k = \gamma_{\text{flip}} = 0$) the optimal interrogation time is $\tau_{\text{int}} = \pi/2\mathcal{J}$, equivalent to a full polarization transfer.

VI. PROBING VIBRATING MOLECULES WITH NANODIAMONDS

As a second application of our general approach we consider an NV center inside a nanodiamond, which is attached to a larger molecule, here the chemokine receptor CXCR4 [23]. The aim is to detect an electron spin label [9] attached to the same molecule in the vicinity of the nanodiamond. There are two main differences from the previous scenario: First, the gyromagnetic ratio of the electron spin is three orders of magnitude larger than that of nuclear spins, which enhances the NV-target coupling considerably. Electron spin labels up to a distance of 10 nm from the NV can therefore be detected. Second, the relaxation time of the NV spin is shorter in nanodiamonds than in bulk diamond because of interactions with surface spins [39].

As for the previous application, we first analyze the stochastic properties of the random thermal motion of the target spin based on ANM simulations. The parameters entering the simulation are the same as in Sec. III A and the structural information of chemokine receptor is obtained from the Protein Data Bank (PDB) [45]. We focus on the impact of molecular motion on the relative distance $\mathbf{r}(t)$ between the NV center and the spin label under the assumption that the nanodiamond is stationary with respect to the external magnetic field. Figure 3 shows representative sample trajectories, obtained from ANM simulations, of the relative distance $\mathbf{r}(t)$ between the NV center and the spin label. The distance $\mathbf{r}(t)$ can be expressed as $\mathbf{r}(t) = \mathbf{R} + \mathbf{q}(t)$, where \mathbf{R} is the equilibrium position and $\mathbf{q}(t)$ represents the thermal fluctuations. The numerical results suggest that $\mathbf{q}(t)$ can be accurately described by an Ornstein-Uhlenbeck (OU) process with the corresponding stochastic differential equation [25]

$$dq_k(t) = -\eta_k q_k(t)dt + \sqrt{2D} dW(t), \quad (21)$$

where the diffusion is assumed to be isotropic and the components $q_k(t)$ are defined with respect to a local orthogonal basis. The restoring force of strength η_k ex-

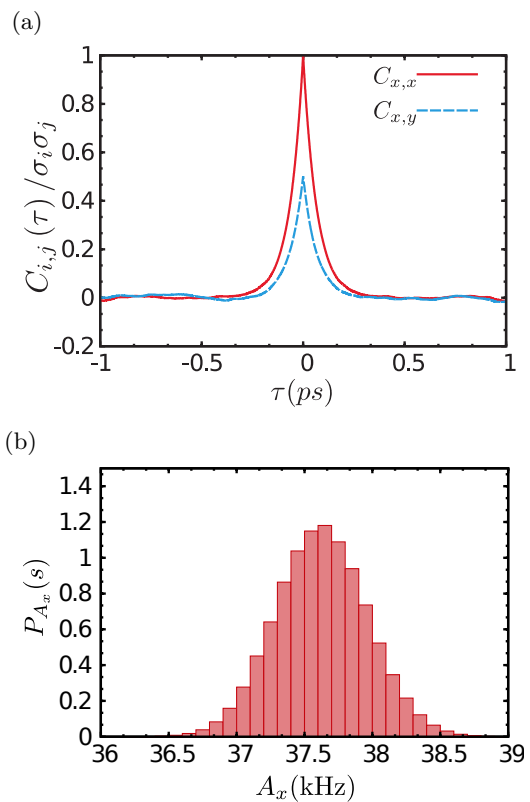


FIG. 8. Characterization of the thermal fluctuations $\xi(t)$ of the hyperfine vector, assumed to be an OU process. (a) The correlations $C_{ij}(\tau)$ are exponentially decaying with typical correlation times $\tau_{ij} \sim 1$ ps. The movement of the spin label is approximately isotropic with comparable correlations in all spatial directions. (b) The distribution $p_{A_x}(s)$ of the x -component of the hyperfine vector $\mathbf{A}(t)$. The approximately Gaussian shape of $p_{A_x}(s)$ is a consequence of the underlying OU process of the fluctuations $\mathbf{q}(t)$.

erted by the molecule acts against the thermal fluctuations which are characterized by the diffusion coefficient \mathcal{D} . The stationary distribution of the fluctuations $q_k(t)$ is Gaussian with variance $\langle \Delta q_k^2(t) \rangle_{\text{tr}} = \mathcal{D}/\eta_k$, whereas $\langle \Delta q_k^2(t) \rangle_{\text{tr}} = 2\mathcal{D}t$ in the regime $t \ll \tau_{\text{exp}}$. We use the two relations to determine the parameters η_k and \mathcal{D} based on numerical estimates of $\langle \Delta q_k^2(t) \rangle_{\text{tr}}$ from the simulations. Typical values obtained in this way are $\eta_k \sim 10$ ps $^{-1}$ and $\mathcal{D} \sim 10^{-5}$ cm 2 s $^{-1}$ for an equilibrium distance $|\mathbf{R}| = 8$ nm and the environment at room temperature.

The distribution $p_{\mathbf{A}}(\mathbf{s})$ and the correlations $C_{ij}(\tau)$ are obtained from the stochastic trajectories $\xi(t)$ of the hyperfine vector, which are generated by numerically solving Eq. (21) with the parameters from ANM simulations and subsequently using the explicit expression for $\mathbf{A}(\mathbf{r})$ in Eq. (2). Figure 8 shows the stationary distribution $p_{A_x}(s)$ and the correlations $C_{ij}(\tau)$. The correlations decay on a time scale $\hat{\tau} \sim 1$ ps such that the condition $\hat{\sigma}^2 \hat{\tau} \ll \tau_{\text{int}}^{-1}$ for the validity of second order cumulant expansion is easily fulfilled. We note that the correlation time is an order of magnitude smaller than in the previ-

ous example. This is to be expected as the correlations $C_{ij}(\tau)$ resulting from an underlying OU process decay on a time scale set by the restoring force η_k rather than by the diffusion coefficient \mathcal{D} [25].

We finally proceed as in Sec. V to determine the interrogation time τ_{int} and total measurement time T required to detect the spin label with unit signal-to-noise ratio. For the realistic values of the coupling $\mathcal{J} = 20$ kHz, the spin flip rate $\gamma_{\text{flip}} = 1$ kHz and $C = 0.03$ we obtain $\tau_{\text{int}} = 0.11$ ms and $T = 0.6$ s. Consequently, the detection of electron spin labels attached to the vibrating chemokine receptor in a thermal environment should be possible in experiments; with the proviso, however, that the rotation of the nanodiamond with respect to the magnetic field is negligible [39].

VII. CONCLUSIONS

In this paper we have shown that detection of single nuclear and electronic spins undergoing diffusion is feasible under realistic experimental conditions by using the Hartmann-Hahn double resonance scheme. Specifically, in the case of rapidly diffusing target spins, which is particularly relevant for experiments at room temperature, we found that the main effect of the diffusion can be absorbed in an effective NV-target coupling. We moreover quantified the decoherence of the NV center induced by the target diffusion, which in the limit of fast diffusion turns out to be significantly smaller than incoherent effects caused by surface magnetic noise.

We emphasize that our approach, namely combining a statistical description of the target diffusion with the quantum description of the spin dynamics, is very versatile. Instead of using ANM simulations for characterizing the statistical properties of the target motion one may use more sophisticated molecular dynamics simulations [26, 27] or, alternatively, rely on experimental data. This is likely to be necessary for setups involving target spins in complex biological environments.

While the main focus of this paper was on spin sensing, our effective model [cf. Eqs. (14) and (15)] is also perfectly suited for analyzing protocols for the polarization of external nuclei by means of optically pumped NV centers [16, 46–50]. This is particularly true for modeling the dynamical polarization of gases and liquids [51], where the diffusive motion of the target spins plays an important role.

ACKNOWLEDGMENTS

The authors acknowledge discussions with F. Jelezko on experimental aspects and H. Plenio on ruthenium based catalysts. This work was supported by an Alexander von Humboldt Professorship, the ERC Synergy grant BioQ and the EU projects SIQS and DIADEMS.

APPENDIX: RELATION BETWEEN DIFFUSION COEFFICIENT AND CORRELATION TIME

We want to clarify the relation between the correlation time of the hyperfine vector $\mathbf{A}(t)$ and the rotational diffusion coefficient \mathcal{D}_r . For simplicity of the argument we consider the scalar case only; the generalization to the vectorial case is based on the same reasoning.

We assume that the hyperfine vector $A(t)$ depends on the quantity $y(t)$, corresponding to $\theta(t)$ or $\varphi(t)$ in the main text, whose evolution is described by a stochastic differential equation of the form

$$dy = \mu(y)dt + \sigma(y)dW. \quad (22)$$

The diffusion term $\sigma(y)$ depends on \mathcal{D}_r as $\sigma(y) \sim \sqrt{\mathcal{D}_r}$ and we assume that the drift term $\mu(y)$ either depends on \mathcal{D}_r as $\mu(y) \sim \mathcal{D}_r$ or is zero. These assumptions are compatible with evolution described by Eqs. (5).

The stochastic differential equation for the hyperfine vector $A(t) = A[y(t)]$ is according to Itô's lemma

$$\begin{aligned} dA(t) &= \left(\mu \frac{\partial A}{\partial y} + \frac{1}{2} \sigma^2 \frac{\partial^2 A}{\partial y^2} \right) dt + \sigma \frac{\partial A}{\partial y} dW \\ &\equiv \tilde{\mu}(A)dt + \tilde{\sigma}(A)dW. \end{aligned} \quad (23)$$

Equation (23) has the same form as Eq. (22) with the diffusion term $\tilde{\sigma}(A) \sim \sqrt{\mathcal{D}_r}$. The drift term in Eq. (23) necessarily depends on \mathcal{D}_r as $\tilde{\mu}(A) \sim \mathcal{D}_r$ except in the trivial case, where $\mu(y)$ is zero and $A(t)$ is simply proportional to $y(t)$.

To determine the correlations of $A(t)$ we need the probability density $p(A, t)$ governed by the Fokker-Planck (FP) equation corresponding to Eq. (23), which is

$$\frac{\partial}{\partial t} p(A, t) = - \frac{\partial}{\partial A} [\tilde{\mu}(A)p(A, t)] + \frac{1}{2} \frac{\partial^2}{\partial A^2} [\tilde{\sigma}^2(A)p(A, t)]. \quad (24)$$

The important observation is that the right-hand side of Eq. (24) is proportional to \mathcal{D}_r such that we can introduce the rescaled time $\tilde{t} = \mathcal{D}_r t$. Using the standard methods for solving the FP equation (24) with reflecting boundary conditions one then obtains for the autocorrelation function [52]

$$\langle A(\tilde{t})A(0) \rangle_{\text{tr}} = \sum_{\lambda} \left[\int dA A P_{\lambda}(A) \right]^2 e^{-\lambda \tilde{t}}, \quad (25)$$

where $P_{\lambda}(A)$ are eigenfunctions with eigenvalues λ of the time-independent FP equation. Thus, we see from Eq. (25) that the correlations of $A(t)$ decay exponentially on a time scale set by \mathcal{D}_r . We note that this result does not apply to the OU process in Eq. (21).

SUPPLEMENTAL MATERIAL

The XYZ file contains the atomic numbers and the Cartesian coordinates of the equilibrium positions of the

constituents of the NHC-Ru complex. The atom used to attach the NHC-Ru complex to the diamond is identified as a helium atom, corresponding to a carbon atom of the diamond surface.

76

6	0.479	-3.582	1.149
6	-0.564	-4.513	1.115
6	-1.087	-4.982	-0.094
6	-0.542	-4.505	-1.289
6	0.502	-3.575	-1.299
6	1.002	-3.130	-0.069
7	1.994	-2.229	-0.059
6	-2.214	-5.987	-0.116
6	3.317	-2.444	-0.046
6	3.947	-1.202	-0.022
6	2.861	1.787	1.146
6	3.011	3.178	1.131
6	3.442	3.856	-0.013
6	3.719	3.114	-1.165
6	3.584	1.722	-1.192
6	3.154	1.075	-0.025
6	2.387	1.087	2.398
6	3.854	0.957	-2.467
7	2.997	-0.255	-0.035
6	3.575	5.358	-0.028
6	1.824	-0.901	-0.051
1	3.749	-3.458	-0.045
1	5.022	-0.958	-0.002
44	0.000	0.000	-0.000
6	1.066	-3.066	-2.605
6	1.017	-3.079	2.468
1	-0.988	-4.886	2.061
1	-0.950	-4.874	-2.245
1	-2.796	-5.956	0.834
1	-2.931	-5.732	-0.931
1	2.776	3.756	2.039
1	4.041	3.646	-2.074
1	1.329	0.761	2.274
1	3.013	0.194	2.622
1	2.434	1.748	3.293

1	4.820	0.409	-2.389
1	3.040	0.226	-2.676
1	3.915	1.629	-3.353
1	4.651	5.643	-0.001
1	3.118	5.785	-0.950
1	3.068	5.834	0.841
1	0.942	-1.961	-2.679
1	2.150	-3.309	-2.682
1	0.561	-3.516	-3.490
1	0.868	-1.978	2.553
1	0.510	-3.550	3.341
1	2.104	-3.300	2.557
7	-1.670	-7.323	-0.298
6	-1.912	-8.060	-1.477
8	-1.410	-9.173	-1.631
2	-2.914	-7.379	-2.740
6	-1.749	-0.740	0.105
6	-2.592	0.461	0.161
6	-1.944	1.732	0.106
6	-2.736	2.880	0.306
6	-4.128	2.782	0.467
6	-4.755	1.526	0.463
6	-3.984	0.362	0.324
9	-4.920	3.985	0.651
8	-0.516	1.888	-0.041
6	-0.091	2.288	-1.366
6	-0.646	1.384	-2.499
6	-0.333	3.790	-1.662
1	-1.073	-7.706	0.404
1	-2.031	-1.743	0.164
1	-2.284	3.828	0.341
1	-5.796	1.456	0.591
1	-4.449	-0.580	0.359
1	-0.176	1.652	-3.447
1	-1.726	1.505	-2.594
1	-0.419	0.340	-2.280
1	0.006	4.391	-0.817
1	-1.390	3.982	-1.844
1	0.233	4.084	-2.549
1	0.993	2.150	-1.373

-
- [1] H. P. Lu, L. Xun, and X. S. Xie, "Single-molecule enzymatic dynamics," *Science* **282**, 1877 (1998).
- [2] O. Flomenbom, K. Velonia, D. Loos, S. Masuo, M. Cotlet, Y. Engelborghs, J. Hofkens, A. E. Rowan, R. J. M. Nolte, M. Van der Auweraer, *et al.*, "Stretched exponential decay and correlations in the catalytic activity of fluctuating single lipase molecules," *J. Proc. Natl. Acad. Sci., U.S.A.* **102**, 2368 (2005).
- [3] K. Velonia, O. Flomenbom, D. Loos, S. Masuo, M. Cotlet, Y. Engelborghs, J. Hofkens, A. E. Rowan, J. Klafter, R. J. M. Nolte, *et al.*, "Single-enzyme kinetics of CALB-catalyzed hydrolysis," *Angew. Chem., Int. Ed.* **44**, 560 (2005).
- [4] M. B. J. Roeffaers, Bert F. S., H. Uji-i, F. C. De Schryver, P. A. Jacobs, D. E. De Vos, and J. Hofkens, "Spatially resolved observation of crystal-face-dependent catalysis by single turnover counting," *Nature* **439**, 572 (2006).
- [5] B. Hulsken, R. Van Hameren, J. W. Gerritsen, T. Houry, P. Thordarson, M. J. Crossley, A. E. Rowan, R. J. M. Nolte, J. A. A. W. Elemans, and S. Speller, "Real-time single-molecule imaging of oxidation catalysis at a liquid-solid interface," *Nat. Nanotech.* **2**, 285 (2007).
- [6] F. Jelezko and J. Wrachtrup, "Single defect centres in diamond: A review," *J. Phys. Status Solidi A* **203**, 3207 (2006).
- [7] T. Staudacher, F. Shi, S. Pezzagna, J. Meijer, J. Du, C. A. Meriles, F. Reinhard, and J. Wrachtrup, "Nuclear magnetic resonance spectroscopy on a (5-nanometer)³ sample volume," *Science* **339**, 561 (2013).
- [8] C. Müller, X. Kong, J.-M. Cai, K. Melentijević, A. Stacey, M. Markham, D. Twitchen, J. Isoya, S. Pezzagna, J. Meijer, J. F. Du, M. B. Plenio, B. Naydenov, L. P. McGuinness, and F. Jelezko, "Nuclear magnetic resonance spectroscopy with single spin sensitivity," *Nature Commun.* **5**, 4703 (2014).

- [9] F. Shi, Q. Zhang, P. Wang, H. Sun, J. Wang, X. Rong, M. Chen, C. Ju, F. Reinhard, H. Chen, *et al.*, “Single-protein spin resonance spectroscopy under ambient conditions,” *Science* **347**, 1135 (2015).
- [10] J.-M. Basset, R. Psaro, D. Roberto, and R. Ugo, *Modern Surface Organometallic Chemistry* (Wiley Online Library, 2009).
- [11] R. Schirhagl, K. Chang, M. Loretz, and C. L. Degen, “Nitrogen-vacancy centers in diamond: nanoscale sensors for physics and biology,” *Annu. Rev. Phys. Chem.* **65**, 83 (2014).
- [12] Y. Wu, F. Jelezko, M. B. Plenio, and T. Weil, “Diamond quantum devices in biology,” Submitted MiniReview for *Angewandte Chemie – International Edition* (2015).
- [13] V. Dragutan, I. Dragutan, L. Delaude, and A. Demonceau, “NHC-Ru complexes-friendly catalytic tools for manifold chemical transformations,” *Coord. Chem. Rev.* **251**, 765 (2007).
- [14] S. Kolkowitz, Q. P. Unterreithmeier, S. D. Bennett, and M. D. Lukin, “Sensing distant nuclear spins with a single electron spin,” *Phys. Rev. Lett.* **109**, 137601 (2012).
- [15] T. H. Taminiau, J. J. T. Wagenaar, T. van der Sar, F. Jelezko, V. V. Dobrovitski, and R. Hanson, “Detection and control of individual nuclear spins using a weakly coupled electron spin,” *Phys. Rev. Lett.* **109**, 137602 (2012).
- [16] P. London, J. Scheuer, J.-M. Cai, I. Schwarz, A. Retzker, M. B. Plenio, M. Katagiri, T. Teraji, S. Koizumi, J. Isoya, R. Fischer, L. P. McGuinness, B. Naydenov, and F. Jelezko, “Detecting and polarizing nuclear spins with double resonance on a single electron spin,” *Phys. Rev. Lett.* **111**, 067601 (2013).
- [17] L. P. McGuinness, L. T. Hall, A. Stacey, D. A. Simpson, C. D. Hill, J. H. Cole, K. Ganesan, B. C. Gibson, S. Praver, P. Mulvaney, F. Jelezko, J. Wrachtrup, R. E. Scholten, and L. C. L. Hollenberg, “Ambient nanoscale sensing with single spins using quantum decoherence,” *New J. Phys.* **15**, 073042 (2013).
- [18] S. R. Hartmann and E. L. Hahn, “Nuclear double resonance in the rotating frame,” *Phys. Rev.* **128**, 2042 (1962).
- [19] J.-M. Cai, F. Jelezko, M. B. Plenio, and A. Retzker, “Diamond-based single-molecule magnetic resonance spectroscopy,” *New J. Phys.* **15**, 013020 (2013).
- [20] M. M. Tirion, “Large amplitude elastic motions in proteins from a single-parameter, atomic analysis,” *Phys. Rev. Lett.* **77**, 1905 (1996).
- [21] P. Doruker, A. R. Atilgan, and I. Bahar, “Dynamics of proteins predicted by molecular dynamics simulations and analytical approaches: Application to α -amylase inhibitor,” *Proteins: Struct. Funct. Genet.* **40**, 512 (2000).
- [22] A. R. Atilgan, S. R. Durell, R. L. Jernigan, M. C. Demirel, O. Keskin, and I. Bahar, “Anisotropy of fluctuation dynamics of proteins with an elastic network model,” *Biophys. J.* **80**, 505 (2001).
- [23] B. Wu, E. Y. T. Chien, Clifford D. M., G. Fenalti, W. Liu, V. Katritch, R. Abagyan, A. Brooun, P. Wells, F. C. Bi, *et al.*, “Structures of the CXCR4 chemokine GPCR with small-molecule and cyclic peptide antagonists,” *Science* **330**, 1066 (2010).
- [24] J.-M. Cai, B. Naydenov, R. Pfeiffer, L. P. McGuinness, K. D. Jahnke, F. Jelezko, M. B. Plenio, and A. Retzker, “Robust dynamical decoupling with concatenated continuous driving,” *New J. Phys.* **14**, 113023 (2012).
- [25] N. G. Van Kampen, *Stochastic Processes in Physics and Chemistry*, 3rd ed. (Elsevier, Amsterdam, 1992).
- [26] B. J. Alder and T. E. Wainwright, “Studies in molecular dynamics. I. General method,” *J. Chem. Phys.* **31**, 459 (1959).
- [27] A. Rahman, “Correlations in the motion of atoms in liquid argon,” *Phys. Rev.* **136**, A405 (1964).
- [28] Q. Cui and I. Bahar, *Normal Mode Analysis: Theory and Applications to Biological and Chemical Systems* (CRC Press, London, 2005).
- [29] D. T. Gillespie, “The mathematics of Brownian motion and Johnson noise,” *Am. J. Phys.* **64**, 225 (1996).
- [30] M. M. Tirado, C. L. Martinez, and J. G. de la Torre, “Comparison of theories for the translational and rotational diffusion coefficients of rod-like macromolecules. Application to short DNA fragments,” *J. Chem. Phys.* **81**, 2047 (1984).
- [31] A. Langer, P. A. Hampel, W. Kaiser, J. Knezevic, T. Welte, V. Villa, M. Maruyama, M. Svejda, S. Jähner, F. Fischer, *et al.*, “Protein analysis by time-resolved measurements with an electro-switchable DNA chip,” *Nat. Commun.* **4**, 2099 (2013).
- [32] A. Langer, W. Kaiser, M. Svejda, P. Schwertler, and U. Rant, “Molecular dynamics of DNA-protein conjugates on electrified surfaces: Solutions to the drift-diffusion equation,” *J. Phys. Chem. B* **118**, 597 (2014).
- [33] See Supplemental Material for the molecular geometry and the atomic numbers of the constituents of the NHC-Ru complex in XYZ file format.
- [34] D. R. Brillinger, “A particle migrating randomly on a sphere,” *J. Theor. Probab.* **10**, 429 (1997).
- [35] R. Kubo, “Stochastic Liouville equations,” *J. Math. Phys.* **4**, 174 (1963).
- [36] F. Petruccione and H.-P. Breuer, *The Theory of Open Quantum Systems* (Oxford University Press, Oxford, 2002).
- [37] Á. Rivas and S. F. Huelga, *Open Quantum Systems. An Introduction* (Springer, Berlin, 2012).
- [38] H. Cramér, “On the theory of stationary random processes,” *Ann. of Math.* **41**, 215 (1940).
- [39] D. Maclaurin, L. T. Hall, A. M. Martin, and L. C. L. Hollenberg, “Nanoscale magnetometry through quantum control of nitrogen-vacancy centres in rotationally diffusing nanodiamonds,” *New J. Phys.* **15**, 013041 (2013).
- [40] T. Roskopf, A. Dussaux, K. Ohashi, M. Loretz, R. Schirhagl, H. Watanabe, S. Shikata, K. M. Itoh, and C. L. Degen, “Investigation of surface magnetic noise by shallow spins in diamond,” *Phys. Rev. Lett.* **112**, 147602 (2014).
- [41] C. P. Slichter, *Principles of Magnetic Resonance*, Vol. 1 (Springer Science & Business Media, New York, 1990).
- [42] Y. Romach, C. Müller, T. Unden, L. J. Rogers, T. Isoda, K. M. Itoh, M. Markham, A. Stacey, J. Meijer, S. Pezzagna, B. Naydenov, L. P. McGuinness, N. Bar-Gill, and F. Jelezko, “Spectroscopy of surface-induced noise using shallow spins in diamond,” *Phys. Rev. Lett.* **114**, 017601 (2015).
- [43] J. M. Taylor, P. Cappellaro, L. Childress, L. Jiang, D. Budker, P. R. Hemmer, A. Yacoby, R. Walsworth, and M. D. Lukin, “High-sensitivity diamond magnetometer with nanoscale resolution,” *Nat. Phys.* **4**, 810 (2008).
- [44] S. F. Huelga, C. Macchiavello, T. Pellizzari, A. K. Ekert, M. B. Plenio, and J. I. Cirac, “Improvement of frequency standards with quantum entanglement,” *Phys. Rev. Lett.*

- 79, 3865 (1997).
- [45] H. M. Berman, J. Westbrook, Z. Feng, G. Gilliland, T. N. Bhat, H. Weissig, I. N. Shindyalov, and P. E. Bourne, “The Protein Data Bank,” *Nucl. Acids Res.* **28**, 235 (2000).
- [46] V. Jacques, P. Neumann, J. Beck, M. Markham, D. Twitchen, J. Meijer, F. Kaiser, G. Balasubramanian, F. Jelezko, and J. Wrachtrup, “Dynamic polarization of single nuclear spins by optical pumping of nitrogen-vacancy color centers in diamond at room temperature,” *Phys. Rev. Lett.* **102**, 057403 (2009).
- [47] J. P. King, P. J. Coles, and J. A. Reimer, “Optical polarization of ^{13}C nuclei in diamond through nitrogen vacancy centers,” *Phys. Rev. B* **81**, 073201 (2010).
- [48] R. Fischer, C. O. Bretschneider, P. London, D. Budker, D. Gershoni, and L. Frydman, “Bulk nuclear polarization enhanced at room temperature by optical pumping,” *Phys. Rev. Lett.* **111**, 057601 (2013).
- [49] Q. Chen, I. Schwarz, F. Jelezko, A. Retzker, and M. B. Plenio, “Optical hyperpolarization of ^{13}C nuclear spins in nanodiamond ensembles,” *Phys. Rev. B* **92**, 184420 (2015).
- [50] E. Rej, T. Gaebel, T. Boele, D. E. J. Waddington, and D. J. Reilly, “Hyperpolarized nanodiamond with long spin relaxation times,” *Nat. Commun.* **6**, 8459 (2015).
- [51] D. Abrams, M. E. Trusheim, D. R. Englund, M. D. Shattuck, and C. A. Meriles, “Dynamic nuclear spin polarization of liquids and gases in contact with nanostructured diamond,” *Nano Lett.* **14**, 2471 (2014).
- [52] C. W. Gardiner, *Stochastic Methods* (Springer-Verlag, Heidelberg, 1985).